Development of thermal joints for conduction-cooling applications

J. Lewis[1*] and G. Ciovati [2,3]

[1] Mechanical & Aerospace Engineering Department, Old Dominion University, Norfolk, USA
[2] Thomas Jefferson National Accelerator Facility, Newport News, VA, USA
[3] Center for Accelerator Science, Physics Department, Old Dominion University, Norfolk, USA

[*]E-mail: jlewi035@odu.edu

Abstract. In support of the development of conduction-cooled superconducting radiofrequency (SRF) niobium cavities for use in continuous-wave linear accelerators, an experimental study of thermal contact resistance was performed on bolted joints using high-purity niobium, aluminium, and copper along with Apiezon N grease and indium foil as interfacial materials. The geometry of each joint investigated aims at replicating the design adopted in conduction-cooled SRF cavities currently under development at Jefferson Lab. The materials' thermal conductivity and the joints' thermal resistance were measured in the temperature range of 3.5 - 10 K. The results showed that the low thermal contact resistance of 2-4 K·cm^2/W at 4.3 K achieved with Al-In-Nb and Al-Apiezon N-Cu joints should allow the operation of conduction-cooled SRF cavities at a targeted accelerating gradient of ~10 MV/m.

1. Introduction

In the development of conduction-cooled superconducting radiofrequency (SRF) linear accelerators [1], bolted joints are commonly employed to facilitate the heat transfer from the cavity to the closed-cycle refrigerators (cryocoolers). A multitude of factors can affect the performance of such thermal joints including the thermal and mechanical properties of the joint materials, surface topography, the use of interfacial materials, and the pressure distribution at the contacting surfaces. The surface resistance of the SRF cavities increases exponentially with temperature, therefore the effectiveness of these joints is characterized by the thermal resistance they impose on the heat flow path across the interface of the joint.

Previous studies on the thermal conductance of pressed metallic contacts at liquid helium temperatures involved joints made of aluminium to niobium [2], copper to copper [3-5], brass to brass [3], aluminium to aluminium [3, 6] and stainless steel to stainless steel [3]. The use of either an indium foil or Apiezon-N thermal grease as thermal interface materials (TIMs), as well as the force applied to the joint have typically been investigated. The results show that the interface thermal conductance, h_c, can be improved significantly by using TIMs. This is understood as TIMs filling microscopic asperities, increasing the effective contact area. For the same type of joint, indium allows using a much lower contact force, compared to Apiezon-N, to achieve similar thermal conductance values. However, a joint where indium has been used at the interface is much more difficult to separate than one in which grease is used. Furthermore, once the joint has been

separated, the removal of the residual indium attached to the surfaces which were in contact may result in scratching of the surfaces, which would require re-work. Previous studies were done on samples with a relatively small contact area, ~1 - 6 cm^2 [2-6], such that the impact of the pressure distribution around a bolted joint might have not been significant. Increasing the contact area of the joint would increase the joint's thermal conductance, however, the pressure distribution over the contact area may become important towards maximizing h_c for bolted joints.

Figure 1 shows a 3D model of a 915 MHz 2-cell SRF niobium cavity designed to operate with conduction-cooling using commercial 4 K cryocoolers [7], along with a schematic representation of the heat flow towards the cryocooler. Bolted joints between the niobium cooling rings/plates, the high-purity aluminium thermal links and the oxygen-free high-conductivity (OFHC) copper flexible thermal links allow transferring the heat generated on the inner surface of the cavity to the second stage of the cryocoolers. Al-Nb and Al-Al joints with indium foil as TIM were successfully adopted for operation of an SRF cavity with conduction-cooling at Fermilab [8, 9], whereas designs with Cu-Cu joints and Apiezon-N or indium as TIM were successfully implemented for SRF cavities at Jefferson Lab [10, 11] and Cornell University [12], respectively. The present study aims at measuring the thermal contact resistance, $R_c = 1/h_c$, of bolted joints that most closely mimic those being designed for the 915 MHz 2-cell SRF cavity. Additionally, the thermal conductivity, κ, of the different materials involved was measured using samples cut from the same batch of materials used to fabricate the sample plates. The results from this study will be implemented into a thermal analysis of the SRF cavity in a cryomodule, to determine the

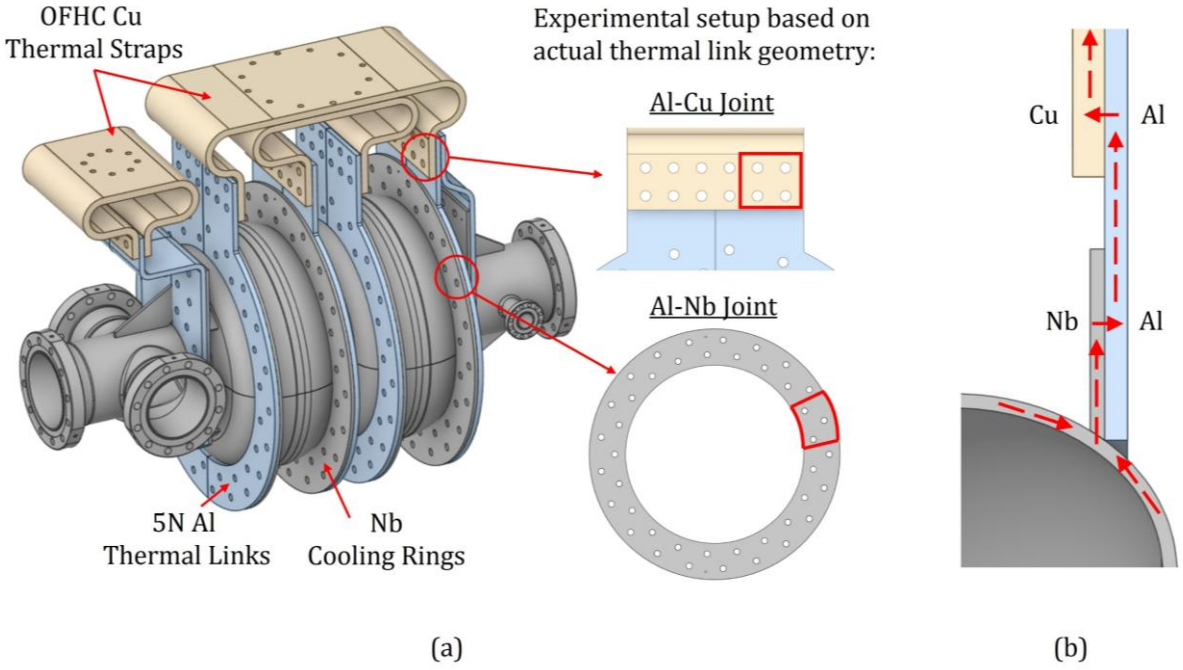

Figure 1. (a) 3D model of 915 MHz 2-cell cavity with Al thermal links and Cu flexible thermal straps, designed to operate with conduction cooling. (b) Cross-section of the cavity showing the heat flow path across the joints.

maximum accelerating gradient that the cavity may achieve, and may be of use for the design of future conduction-cooled systems operating at ~4 K.

2. Experimental setup

2.1 Samples preparation

Five plates for R_c measurements were cut by wire-electro-discharge machining (wire-EDM) from a larger 6.35 mm thick plate of 99.999% (5N) pure aluminium. Three plates had three bolt holes machined, each 8.4 mm in diameter with a centre-to-centre spacing of 3 cm in a staggered pattern. Two plates had four bolt holes, each 8.4 mm in diameter uniformly spaced 2.54 cm centre-to-centre. The plates were etched in a "pickling" solution of HNO_3:HF:H_2O = 25:1:74 by volume at 25 °C for 30 min.

A niobium plate for R_c measurements was also cut by wire-EDM from a 4 mm thick larger plate of high purity Nb, with residual resistivity ratio (RRR) > 250. Three and four-holes bolt patterns, matching that of the Al plates, were machined in the Nb plate. The plate was etched by buffered chemical polishing (BCP) with a mixture of HF:HNO_3:H_3PO_4 = 1:1:2 by volume to remove ~20 μm.

A 9.525 mm thick base plate connecting the Al and Nb plates to a cryocooler adapter disc was machined from a half-hard OFHC Cu plate. Four-holes bolt patterns matching that of the Nb and Al plates and an eight-hole circular bolt pattern matching that of the cryocooler adapter disc were machined in the plate. Tapped holes, 2.84 mm in diameter were machined at specific locations in all plates to allow mounting of the cryogenic temperature sensors. After machining, the Cu plate was etched with a “bright dip” solution of H_2O:H_2SO_4:HNO_3:HCl = 49:43:7:1 by volume, at 25 °C for 10 min.

Table 1 summarizes the plates’ dimensions, contact area, A_c, flatness and average surface roughness, R_a. The flatness of the contact area was measured with a laser scanning coordinate measuring machine in which the flatness is reported as the deviation between the highest and lowest measured points relative to a best-fit plane on the surface of the plate. The surface roughness of the contact area was measured with a stylus profilometer.

The thermal conductivity of the Cu plate was obtained directly during the thermal resistance tests described in the section 3.2. Aluminium and Nb samples with ~3 mm × ~2 mm cross-section, 120 mm long, were cut by wire-EDM from the same material used to prepare the plates listed in Table 1, for thermal conductivity measurements. One of the Al samples was bent at 90° in four places, forming a "U"-shape towards the middle of the sample, to investigate the impact of strain on κ. The bending radii were 3 - 5 mm resulting in ~25% local strain. The Al samples have been etched with HNO_3:HF:H_2O = 25:1:74 by volume at 25 °C for 1 h, removing ~15 μm. The Nb sample was etched by BCP removing ~50 μm followed by vacuum annealing at 450 °C for 3 h and 800 °C for 3 h. The sample was etched by BCP removing ~20 μm after annealing.

2.2 Joint configurations

We have investigated the thermal contact resistance of the following bolted joints configurations among the plates described in section 2.1:

Table 1. Overall dimensions, contact area, flatness and surface roughness of the sample plates used for the thermal contact resistance measurements. The flatness and R_a values in the top and bottom rows for the Nb and Cu plates are those for the top and bottom contact surfaces, respectively.

Plate ID	Width × Length × Thickness (mm^3)	A_c (cm^2)	Flatness (μm)	R_a (μm)
Al 1	50.8 × 120.7 × 6.4	37.0	40	0.73 ± 0.08
Al 2	50.8 × 120.7 × 6.4	37.0	73	0.25 ± 0.08
Al 3	50.8 × 120.7 × 3.2	37.0	67	0.22 ± 0.08
Al 4	50.8 × 94.0 × 6.4	23.5	33	0.82 ± 0.08
Al 5	50.8 × 94.0 × 3.2	23.5	148	0.37 ± 0.08
Nb	50.8 × 146.1 × 4.0	37.0	131	0.63 ± 0.08
			133	0.61 ± 0.08
		23.5	91	0.57 ± 0.08
Cu	50.8 × 222.3 × 9.5	23.5	26	0.11 ± 0.08
			82	0.14 ± 0.08

1. Al-Nb joint with 0.127 mm thick, 99.99% In foil as TIM, a stack of three oversized (26.6 mm OD, 13.3 mm ID, 2.5 mm thick) stainless steel 316 flat washers on both sides of the joint. 5/16"-24 stainless steel A286, twelve-point bolts and silicon-bronze nuts torqued to 21.7 N·m (16 ft·lbs). Two Inconel Belleville washers (17.5 mm OD, 8.8mm ID, 1.25mm thick) stacked in parallel were placed between the bolt heads and the flat washers.
2. Al-Nb joint, same as configuration No.1 but with 6.35 mm thick Al 7075 backing plates replacing the flat washers on both sides of the joint.
3. Al-Nb joint, same as configuration No. 2 but with Apiezon-N replacing the In foil and with torque applied to the bolts increased to 48.8 N·m (36 ft·lbs).
4. Nb-Cu joint with Apiezon-N as TIM, 6.35 mm thick stainless steel 304 backing plates. 5/16"-24 stainless steel A286, twelve-point bolts and silicon-bronze nuts torqued to 48.8 N·m. The torque value was reduced to 39.3 N·m (29 ft·lbs) in a subsequent test.
5. Al-Cu joint, same as configuration No. 4. 5/16"-24 stainless steel A286, twelve-point bolts and silicon-bronze nuts torqued to 48.8 N·m.

Figure 2 shows 3D models of the various joint configurations. For joints where In was used as TIM, the bolts were torqued three times to the target value, at 8 h intervals, to compensate for the creep of the soft indium foil.

The pressure distribution over the contact area for each joint configuration was measured at room temperature using Fujifilm's Prescale pressure measurement film. The colour density of the film was digitized and converted to pressure using the manufacturer's data sheets and OriginPro software. The pressure maps are shown in figure 3. A higher and more uniform pressure was achieved for the Al-Cu and Nb-Cu joints, compared to the Al-Nb joint, because of the higher torque

of the bolts and the use of stainless-steel backing plates. In a previous study on Nb-Al joints with indium as TIM, it was found that the thermal contact resistance was weakly dependent on the contact pressure, above the nominal compressive yield strength of indium of ~2.14 MPa [2]. Analysis of the pressure distribution plots shown in figure 3(a)-(b) shows that the contact pressure is above 2.14 MPa over ~60% of the contact area and that no significant difference in pressure distribution was found between using oversized washers compared to Al 7075 backing plates. Al 7075 was chosen instead of stainless steel as the material for the backing plates for the Al-Nb joint because of the reduced weight and non-magnetic properties of Al, which are important for materials used in closed proximity to an SRF cavity.

High contact pressure is beneficial to achieving low thermal contact resistance when using Apiezon-N as TIM, possibly due to the fact that, unlike indium, Apiezon-N becomes rigid at cryogenic temperatures and might actually separate the contact surfaces, unless a high pressure is applied to the joint at room temperature [3]. Bolts with silicon bronze nuts of the same type as those used in the setup were found to yield at ~74 N·m, ~52% higher than the applied torque.

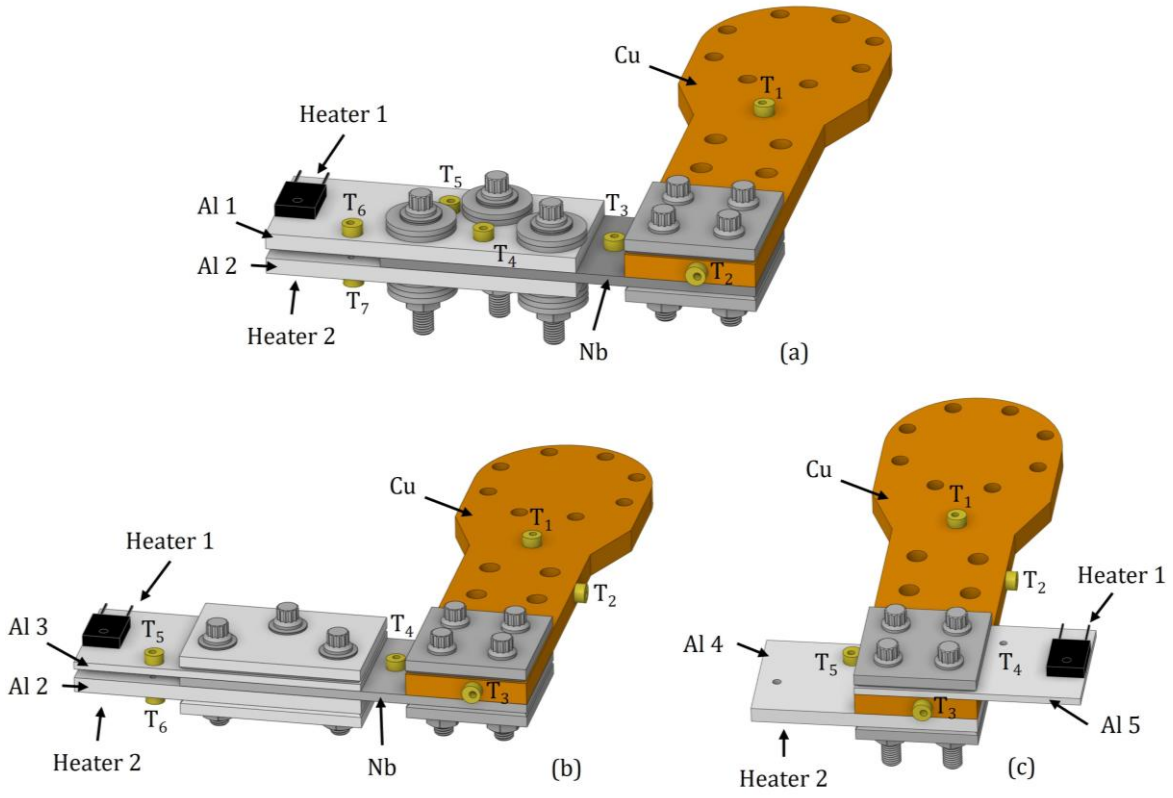

Figure 2. 3D models of the different test assemblies used for measuring the thermal contact resistance of joint configurations. With reference to the text, (a) is related to joint configurations 1 and 4; (b) is related to joint configurations 2, 3, and 4 and (c) is related to joint configuration 5.

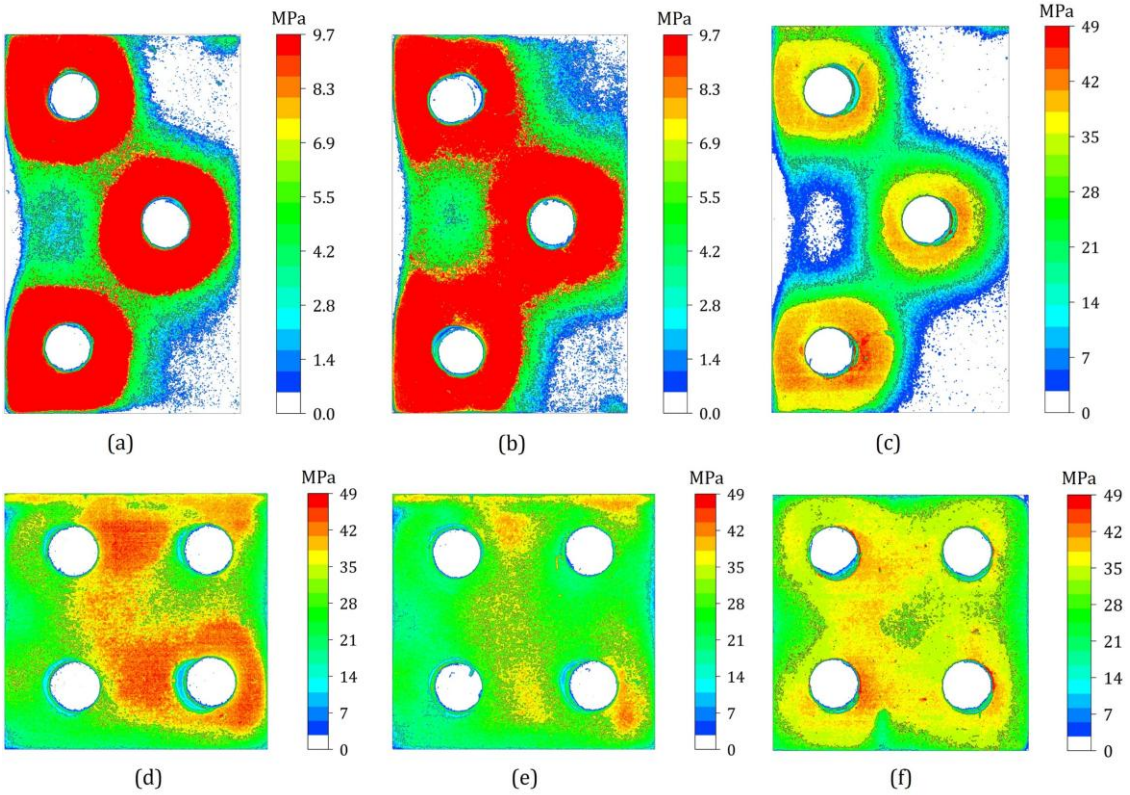

Figure 3. Pressure distribution measured for each joint configuration: (a) Al 2-Nb, washers, 21.7 N·m; (b) Al 2-Nb, Al 7075 backing plates, 21.7 N·m; (c) Al 2-Nb, Al 7075 backing plates, 48.8 N·m; (d) Nb-Cu, stainless steel backing plates, 48.8 N·m; (e) Nb-Cu, stainless steel backing plates, 39.3 N·m; (f) Al 4-Cu, stainless steel backing plates, 48.8 N·m.

2.3 Thermal resistance measurement setup

The setup with the joints' configurations discussed in section 2.1 is mounted to an OFHC Cu adapter disc, mounted to the second stage of a commercial Gifford-McMahon cryocooler (RDE418-D4, SHI Cryogenics Group) with a nominal cooling power of 2.0 W at 4.2 K and mounted to a vertical test stand. Apiezon-N was used as TIM at top and bottom round contact surfaces of the adapter disc. Prior to bolting of the joints, the surface of the plates was wiped with isopropanol and lint-free wipes. The indium foil was cleaned with lint-free wipes soaked in acetone first and isopropanol last.

Calibrated cryogenic temperature sensors (Cernox CX-1050-CU, Lake Shore Cryotronics) were mounted to the plates as recommended by the manufacturer. Manganin wires, 0.127 mm in diameter (WQL-36, Lake Shore Cryotronics), ~3 m long extend the temperature sensors' leads to a vacuum feedthrough on the top plate of the vertical test stand. Copper wires, 0.254 mm in diameter, connect two non-inductive heaters (LTO 100, Vishay, 25 Ω ± 1%) to another vacuum feedthrough. The heaters are mounted to the Al plates using a mounting screw, washer and Apiezon-N as TIM. All wires are thermally intercepted to the 1st stage of the cryocooler. The heat leak of the sensors and heaters wires from the 40 K 1st stage to the test specimen at 4 K is estimated to be < 100 nW and ~7 μW, respectively.

After installation of the temperature sensors and heaters, the setup is wrapped with twelve layers of multi-layer insulation. A copper cylinder, connected to the cryocooler's 1st stage, serves as the thermal shield. Figure 4 shows the experimental setup at various stages of the assembly. The test stand is inserted in a vertical dewar and evacuated to ~1×10^{-4} mbar prior to cool-down. Current to the heaters is provided with a power supply (E36313A, Keysight) and a temperature monitor (Model 18i, Cryogenic Control Systems) is connected to the temperature sensors' wiring. A LabVIEW software is used to control the instruments and for the data acquisition.

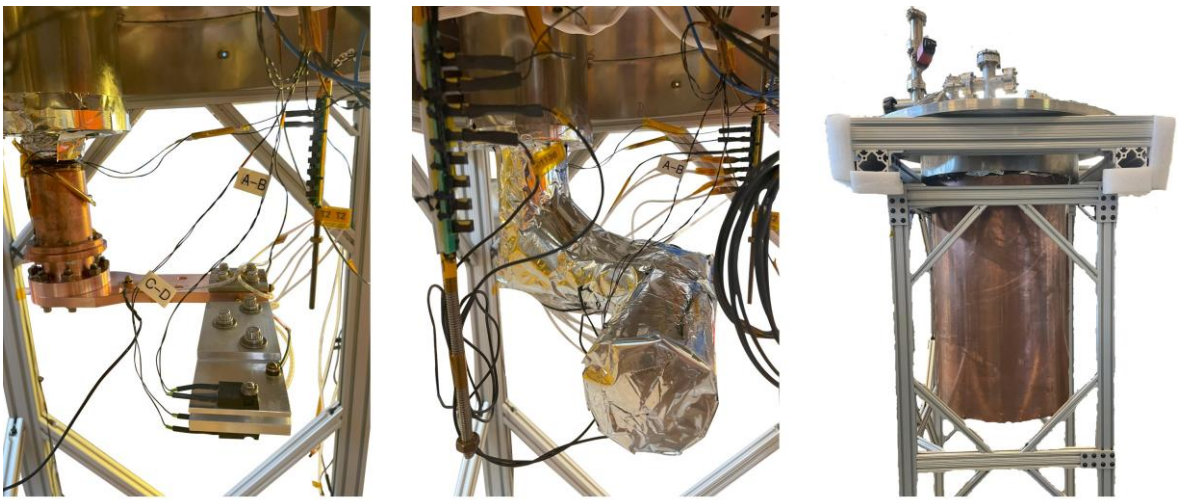

Figure 4. Pictures of the experimental setup for R_c measurements: (a) sample plates mounted to the cryocooler's 2nd stage, (b) multi-layer insulation wrapped around the setup and (c) vertical test stand with thermal shield.

2.4 Thermal conductivity measurement setup

The thermal conductivity experimental setup follows the axial flow configuration [13] and it is shown in figure 5. The sample is subjected to a temperature-controlled cold sink on one end and a thermal load on the other. Temperature sensors are then fixed to the specimen between the load and sink at a measured distance apart.

One end of the sample is clamped to an OFHC Cu bar protruding through a stainless steel vacuum flange. A heater made by wrapping constantan wire, epoxied to a OFHC Cu mount, is clamped on the opposite end of the sample. Two similarly mounted calibrated cryogenic temperature sensors (Cernox CX-1030-SD, Lake Shore Cryotronics), are clamped to the sample between the hot and cold sides. Indium foil is used as TIM for all the connections to the sample. The distance between temperature sensors is measured with a digital calliper, the samples cross-section is measured with a digital micrometre at three locations along the sample.

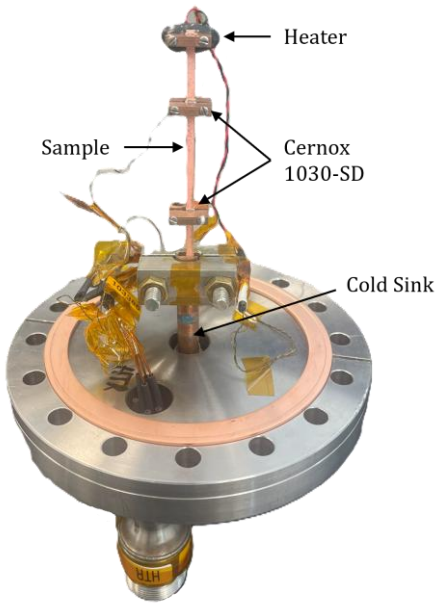

Figure 5. Picture of part of the experimental setup used to measure the thermal conductivity.

The flange with the setup is bolted to a small vacuum chamber, assembled to a vertical test stand. The vacuum chamber is evacuated to ~1×10^{-5} mbar prior to cool-down. The test stand is inserted in a vertical dewar which is filled with liquid helium at 4.3 K. The temperature inside the cryostat is lowered to ~2 K by pumping on the helium bath. A current source (Model 2200-32-3, Keithley Instruments) and nanovolt meter (Model 2182, Keithley Instruments) are used to supply the current and measure the voltage to the heater, respectively. A temperature monitor (Model 218, Lake Shore Cryotronics) is used to measure the temperature from the temperature sensors. A LabVIEW software is used to control the instruments and for the data acquisition.

3. Experimental results

3.1 Thermal conductivity

The thermal conductivity as a function of temperature was calculated from the measured heater power, P, steady-state temperature difference, ΔT, distance between temperature sensors, d, and cross-section area, S, as:

$$\kappa(T) = \frac{P}{\Delta T}\frac{d}{S}. \quad (1)$$

The thermal conductivity of the Cu plate was calculated from temperature difference between sensors T_1 and T_2, shown in figure 2(b), for each power level applied to each of the heaters, also shown in figure 2(b). The final data set is the weighted average of multiple sets of data.

A plot showing the thermal conductivity of the Al, Nb and Cu materials used in the thermal contact resistance setup is shown in figure 6. The thermal conductivity at 4.3 K of the strained sample was ~12% lower than the unstrained one. After the initial test, the Al samples were heat treated at 200 °C for 1 h in a vacuum furnace, etched for 30 min with the HNO_3:HF:H_2O = 25:1:74 solution and re-tested. The thermal conductivity at 4.3 K of both bent and straight samples

increased significantly after annealing. The bent sample was straightened to its initial shape and re-tested, showing a ~20% reduction in the thermal conductivity at 4.3 K.

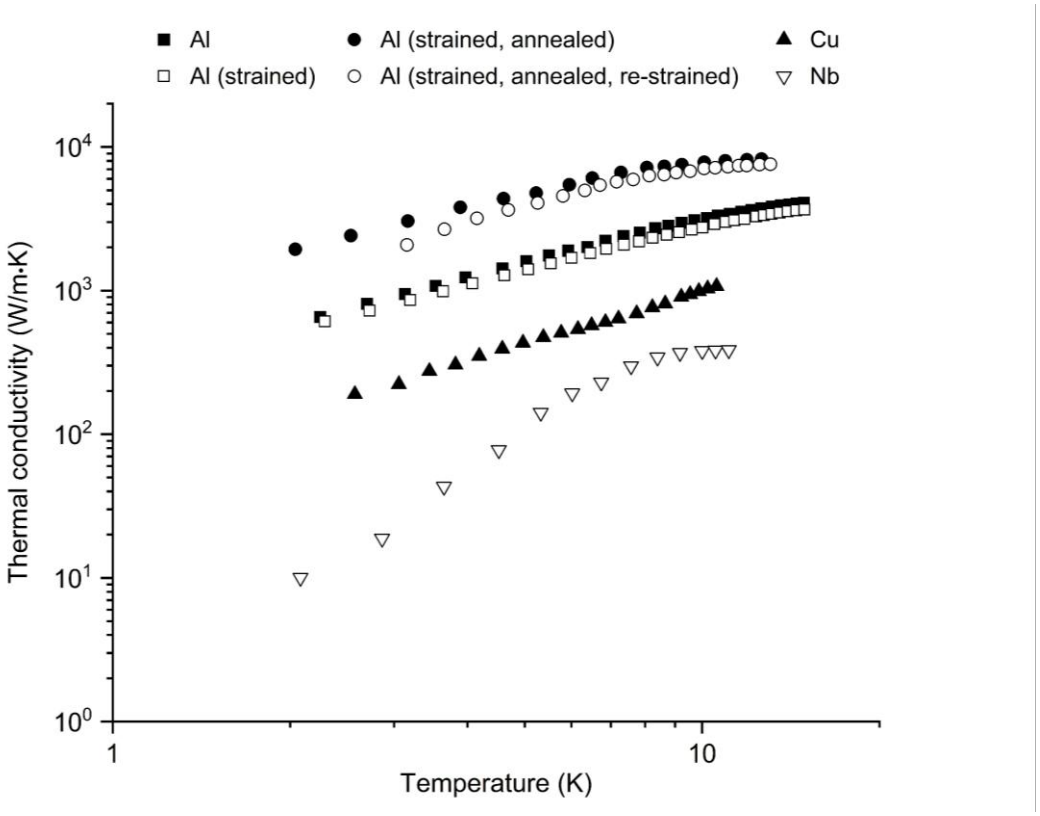

Figure 6. Thermal conductivity of the materials used for the thermal contact resistance measurements. The size of the error bars is smaller than the size of the symbols.

The thermal conductivity of the Cu plate and Al samples was fit with empirical formulas to obtain the materials' RRR values [13]. The RRR of the Nb sample was calculated using the approximate relation to κ, RRR ≅ 4· κ(4.3 K) [14]. The values of κ(4.3 K) and RRR for the Al, Cu and Nb are listed in Table 2. The Cu plate was machined from material acquired from a general industrial supplier and the RRR value is consistent with those reported from recent tests on samples machined from material provided by a variety of vendors [15].

Table 2. Thermal conductivity of Nb and Al samples and of the Cu plate used for the thermal contact resistance measurements.

Material	κ(4.3 K) [W/(m·K)]	*RRR*
Al	1290 ± 61	324 ± 3
Al, heat treated	4211 ± 270	980 ± 4
Nb	80 ± 3	319 ± 12
Cu	386 ± 47	51 ± 2

3.2 Thermal contact resistance

Upon each cool-down, the steady-state temperature of the Cu plate was ~2.4 K and the pressure in the cryostat was ~1.5×10^{-6} mbar. The test procedure consisted of setting the current to the heater in the top Al plate, waiting for all temperature sensors in the setup to reach steady-state conditions ($\mathrm{d}T/\mathrm{d}t$ < 0.25 mK/min) and measuring the temperature from all sensors and the heater's current and voltage. The heater current is then increased and the procedure is repeated, covering values of the average temperature of the joints in the range of 3 - 10 K. The heater current is then turned off and the setup is allowed to cool to its initial temperature. The test procedure is repeated using the heater on the bottom plate, matching the same power as when the top heater was powered, measuring the temperature from all sensors after reaching steady-state conditions for each power level.

The procedure described above allows calculating the temperature difference across the Al-Cu joints or Nb-Al joints using the same temperature sensor, following the "two-heater" method [2, 16]. As an example, the thermal contact resistance for the joint between the top Al plate and the Nb plate is calculated as:

$$R_c(T) = \frac{T_{Al,hot} - T_{Al,cold}}{P}, \quad (2)$$

where $T_{Al,hot}$ is the temperature of the top Al plate when the top heater is powered and $T_{Al,cold}$ is the temperature of the top Al plate when the bottom heater is powered with the same power, P.

On the other hand, the temperature difference across the Nb-Cu joint can only be calculated from the temperatures measured directly on the Nb and Cu plates. In this case, the temperature across the joint is corrected for the distance between the sensor on the Nb plate and the edge of the joint and for temperature offsets when no power is applied to the heaters, as follows:

$$\Delta T_{corr}(P) = T_{Nb}(P) - T_{Nb}(0) - \Delta T_{Nb}(P) - T_{Cu}(P) + T_{Cu}(0), \quad (3)$$

where $\Delta T_{Nb}(P)$ is calculated as:

$$\Delta T_{Nb}(P) = \frac{P}{\kappa(T)} \frac{d_{Nb}}{S_{Nb}}. \quad (4)$$

d_{Nb} = 9.5 mm is distance between the centre of the temperature sensor and the edge of the joint and S_{Nb} = 2 cm^2 is the cross section of the Nb plate. The thermal conductivity is taken at the temperature measured by the sensor, linearly interpolated from the data measured on the Nb sample. The temperature sensor in the Cu plate is mounted directly under the joint, therefore a similar correction is not necessary.

Figures 7 and 8 show the thermal contact resistance as a function of temperature, for the three configurations of the Al-Nb joints, and the Nb-Cu and Al-Cu joints, respectively. The thermal contact resistance values shown in figures 7 and 8 are the weighted average of two test cycles. The different test configurations are listed in section 2.2.

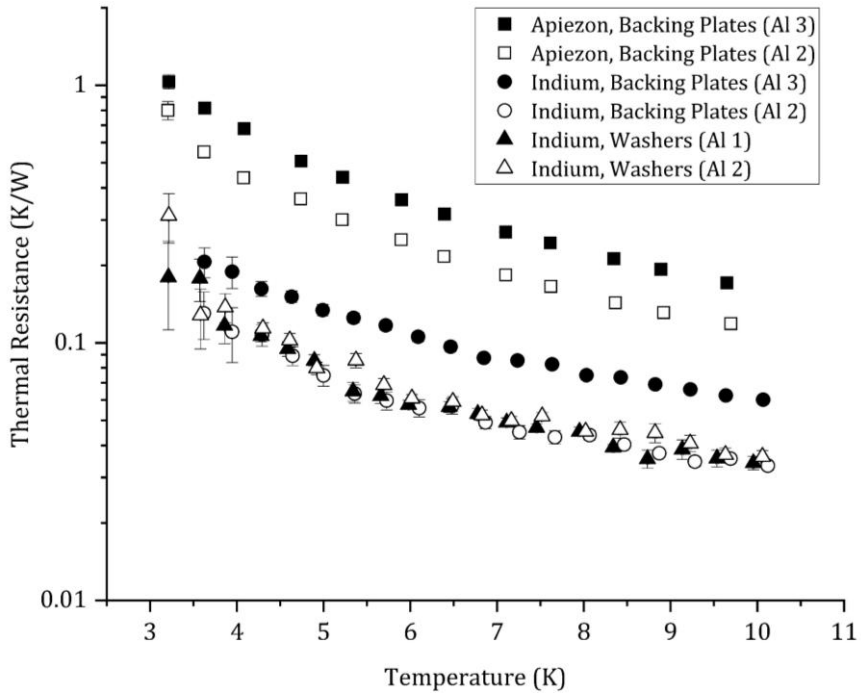

Figure 7. Thermal contact resistance as a function of temperature for different Al-Nb bolted joints configurations. The contact area is 37.0 cm^2. Error bars which are not visible are smaller than the size of the markers.

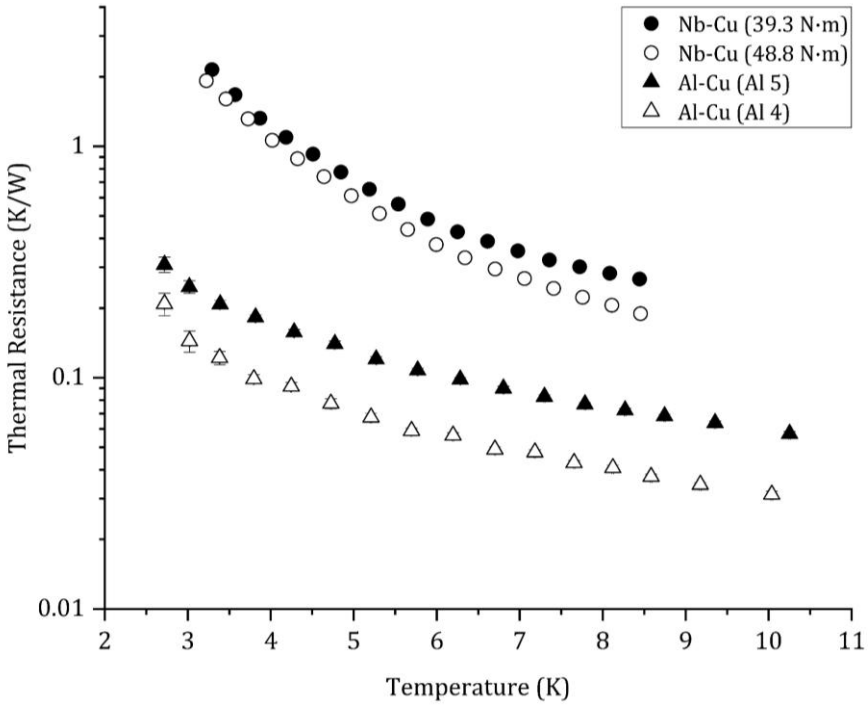

Figure 8. Thermal contact resistance as a function of temperature for Nb-Cu and Al-Cu bolted joints with Apiezon-N as TIM, backing plates and different torque values. The contact area is the same for both joints and equal to 23.5 cm^2. Error bars which are not visible are smaller than the size of the markers.

4. Discussion

The design and implementation of thermal links with low thermal contact resistance is an important aspect of developing conduction-cooled SRF cavities for particle accelerators. It is well-established that the use of TIMs enhances heat conduction through interfaces at cryogenic temperatures. The results presented in this study show that a lower R_c for the Al-Nb joint was obtained when using In as TIM, instead of Apiezon-N, which is consistent with the previous results measured at Fermilab [17]. The results on Al-In-Nb joint also show that there was no significant difference in the thermal contact resistance values at 4.3 K when using oversized stainless steel washers than an Al 7075 backing plate, consistently with the similar pressure distribution maps. The thermal resistance of the Al-In-Nb joint at 4.3 K from the present study is only a factor of ~1.8 lower than that achieved in a joint using the same materials, at about the same temperature and with an estimated contact pressure of 12 MPa, as reported in Ref. [2], in spite of the apparent contact area being a factor ~6.3 greater than that of Ref. [2]. This may be a result of a significant fraction of the apparent contact area having low contact pressure in the larger joint configuration, as seen from the pressure maps in figure 3(a)-(b).

Table 3. Total thermal contact resistance at ~4.3 K for different joints configurations from measured temperatures and power.

Joint	R_c (K/W)
Al 1-In-Nb (washers)	0.11 ± 0.01
Al 2-In-Nb (washers)	0.10 ± 0.01
Al 3-In-Nb (backing plates)	0.16 ± 0.01
Al 2-In-Nb (backing plates)	0.11 ± 0.01
Al 3-Apiezon-Nb	0.62 ± 0.01
Al 2-Apiezon-Nb	0.41 ± 0.01
Al 4-Cu	0.09 ± 0.004
Al 5-Cu	0.15 ± 0.004
Nb-Cu, 48.8 N·m	0.88 ± 0.01
Nb-Cu, 39.3 N·m	1.03 ± 0.02

The Al-Cu joint with Apiezon-N as TIM and the Al-Nb joints with indium foil as TIM showed the lowest thermal contact resistance. The use of Apiezon-N as TIM in the Al-Nb joint showed a higher thermal contact resistance compared to the use of indium foil as TIM for the same configuration. The Nb-Cu joint with the same configuration and TIM as the Al-Cu joint showed a significantly higher thermal contact resistance. Additionally, reducing the torque value of the bolts for the Nb-Cu joint with Apiezon-N by 20% resulted in an increase of the thermal contact resistance.

The results also show that R_c is significantly higher for joints with the thinner Al plate than the same ones with thicker Al plate. In the case of the Al 5-Cu joint, it was noticed that the pressure distribution had greater non-uniformity compared to that of the Al 4-Cu joint and that Al 5 has significantly worse flatness than that of Al 4. The possible cause for the higher R_c of the Al-Nb joint with the thinner Al plate, compared to the one for the thicker Al plate is unclear.

Measurements on a conduction-cooled SRF cavity operating up to an accelerating gradient of ~12 MV/m with two Cu-Apiezon N-Cu thermal joints between the cavity and each cryocooler indicated a thermal resistance of ~4 K·cm^2/W at 4 K for each joint [11]. The results on Al-In-Nb and Al-Apiezon N-Cu joints in Table 3, showing a thermal resistance of ~4 K·cm^2/W and ~2 K·cm^2/W, respectively, are comparable to that of the joint that was already used in operation of a conduction-cooled cavity.

In terms of cost and complexity of the joint assembly, Apiezon N is more favourable than indium as TIM. Apiezon N is radiation-resistant, whereas radioactive isotopes of Indium may be formed by direct impact of electron with energy above 15 MeV. However, such beam energy is above the 10 MeV value commonly targeted by conduction-cooled SRF accelerators for industrial applications. The concern about long-term creep of the indium, possibly causing an increase of thermal contact resistance over time, is mitigated by the multiple re-torqueing of the bolted joint after 8 h time intervals. This procedure was established for the assembly of thousands of Nb-In-Nb hermetical joints for SRF cavities operating below 4 K in the CEBAF accelerator [17].

5. Summary and conclusions

In this study we investigated the thermal contact resistance of different bolted joints configurations, with a large contact area, mimicking those designed for conduction-cooled SRF cavities that are being developed at Jefferson Lab. The thermal contact resistance at 4.3 K was the lowest for Al-Nb joints with In as TIM and the Al-Cu joint with Apiezon N as TIM. The thermal contact resistance at 4.3 K was the highest for Al-Nb and Nb-Cu joints with Apiezon N as TIM. No significant difference was found in the thermal contact resistance of the Al-Nb joints when using backing plates versus washers. The pressure distribution over the large contact surfaces is non-uniform, which could result in a non-uniform thermal contact resistance. A much higher contact pressure was applied to the joints where Apiezon-N was used as TIM and no significant difference in the thermal contact resistance of the Nb-Cu joint was found when the bolt torque was changed by ~20%.

In conclusion, bolted-joint configurations consisting of Al-In-Nb and Al-Apiezon N-Cu with thermal contact resistance values of 2 - 4 K·cm^2/W at 4.3 K have been developed for thermal links to be used for the operation of a conduction-cooled SRF cavity. The results from this study will be used for the thermal analysis of 915 MHz conduction-cooled SRF cavities, determining the maximum accelerating gradient and the corresponding heat flux generated at the cavities' inner surface that can be removed by crycoolers.

Acknowledgments

We would like to thank B. Khanal and Dr. Tian-Bing Xu of ODU for assisting at various points in the study. At Jefferson Lab, we would like to thank J. Kent and A. Malave-Colon for helping with cryogenic operations, S. Dutton for assistance with temperature sensors' installation and the SRF Cavity Production Group for helping with the surface treatments of the samples. We would also like to thank R. Dhuley of Fermilab, G. Cheng of Jefferson Lab and T. Schultheiss of TJSTechnologies for many useful discussions. This material is based upon work supported by the U.S. Department

of Energy (DOE), Office of Science, Office of Nuclear Physics under contract DE-AC05-06OR23177. J. L. was supported in part by DOE Traineeship Grant DE-SC0022309 to ODU and by the Accelerator Stewardship program within the DOE Office of Accelerator R&D and Production.

References

[1] Padamsee H 2009 *RF Superconductivity: Science, Technology, and Applications* (Weinheim: Wiley-VCH).
[2] Dhuley R C, Geelhoed M I and Thangaraj J C T 2018 *Cryogenics* **93** 86.
[3] Salerno L J, Kittel P and Spivak A L 1994 *Cryogenics* **34**, 649.
[4] Dillon A, McCusker K, Van Dyke J, Isler B and Christiansen M 2017 Thermal interface material characterization for cryogenic electronic packaging solutions *IOP Conf. Ser.: Mater. Sci. Eng*. **278** 012054.
[5] Dhuley R C 2019 *Cryogenics* **101** 111.
[6] Dhuley R C et al 2019 *IEEE Trans. Appl. Supercond.* **29** 0500205.
[7] Ciovati G et al 2024 RF and mechanical design of a 915 MHz SRF cavity for conduction-cooled cryomodules *Proc. LINAC2024* 732-735. doi:10.18429/JACoW-LINAC2024-THPB046.
[8] Dhuley R C, Posen S, Geelhoed M I, Prokofiev O and Thangaraj J C T 2020 *Supercond. Sci. and Technol*. **33** 06LT01.
[9] Dhuley R C et al 2022 Development of a cryocooler conduction-cooled 650 MHz SRF cavity operating at 10 MV/m CW accelerating gradient *IOP Conf. Ser.: Mater. Sci. Eng*. **1240** 012147.
[10] Ciovati G, Cheng G, Pudasaini U and Rimmer R A 2020 *Supercond. Sci. Technol*. **33** 07LT01.
[11] Ciovati G et al 2023 *Phys. Rev. Accel. Beams* **26**, 044701.
[12] Stilin N A et al 2023 *Eng. Res. Express* **5** 025078.
[13] Hust J G and Lankford A B 1984 Thermal conductivity of aluminum, copper, iron and tungsten for temperatures from 1 K to the melting point National Bureau of Standards, Boulder, CO, NBSIR 84-3007.
[14] Padamsee H, Knobloch J and Hays T 2008 *RF Superconductivity for Accelerators* (Weinheim: Wiley-VCH).
[15] Valois J J, Nellis G F and Pfotenhauer J M 2024 *IOP Conf. Ser.: Mater. Sci. Eng.* **1301** 012167.
[16] Didschuns I, Woodcraft A L, Bintley D and Hargrave P C 2004 *Cryogenics* **44** 293.
[17] C W Leemann, D R Douglas and G A Krafft 2001 The Continuous Electron Beam Accelerator Facility: CEBAF at the Jefferson Laboratory *Annu. Rev. Nucl. Part. Sci.* **51** 413–450.
[18] Dhuley R C 2024 private communication.